Synchrotron tomography on zinc and aluminium foams

A. Rack, A. Haibel, B. Matijasevic and **J. Banhart**
Materials Science Dept., Hahn-Meitner-Institut Berlin, Germany

We report on synchrotron tomography on zinc and aluminium foams. Using three dimensional image analysis critical cell wall thicknesses and distribution functions for both the blowing agent and the pore size are determined. For Al foams stabilised with SiC particles correlation functions of SiC particles with pores are determined and discussed.

1 Introduction and methods

Synchrotron radiation tomography as one of the most sophisticated non-destructive imaging methods has been shown to be perfectly suited for investigating metallic foams [1]. High resolution studies can be performed on foams in early and late expansion stages. Using monochromatic radiation one can collect information not only about the mass distribution within the sample, but also about the element distribution.

Zinc foam samples were produced using the powder compact foaming process [2]. Pure zinc is mixed with 0.5 vol-% TiH_2 or, alternatively, 0.66 vol-% ZrH_2 to form two different series of zinc foams. By heating in a furnace including the possibility of interrupting the foaming process by rapid cooling at any time we create zinc foams with different porosities P.

Aluminium alloy AlSi10Mg foam stabilised with 10 vol.% SiC is produced using a cast solid precursor, manufactured by the metal foam group at the University of Cambridge (UK) [3].

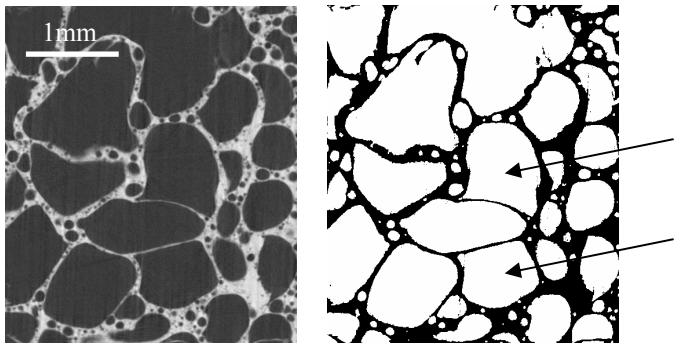

Fig. 1. Tomographic slice of zinc foam (left) with P = 72% and corresponding Boolean image carrying only the pore information (right), arrows denote typical large final-stage pores

Tomographic images were obtained at the BAMline (BAM – Federal Institute of Materials Research and Testing, Germany) located within BESSY II (Berlin electron storage ring company for synchrotron radiation, Germany) with resolutions of 5.4 µm and 10.8 µm using energies of 25 keV (aluminium foam) and 60 keV (zinc foam).

In order to separate the information in one 3D dataset (see, e.g., Fig. 1, left image) which belongs to different morphological objects (pores, metal matrix, blowing agents etc.) a growth algorithm is used. Growth means, e.g. for pores, that all voxels with grey values below a *threshold1* are used as initial points from where in successive stages all next neighbours are collected with a value below a *threshold2*. These so-called Boolean images (only containing ones and zeros – see Fig. 1, right image) are used for further analysis: with 3D dilatation of the pores information is collected about how much SiC can be found at which distance to the pores. A plot of the differential (value of the current step minus value of the previous step) SiC density found within each dilatation step vs. normalized dilated volume (see Fig. 6) displays correlation (decreasing SiC density) or non-correlation (constant SiC density) or even anti-correlation (increasing SiC density) [4].

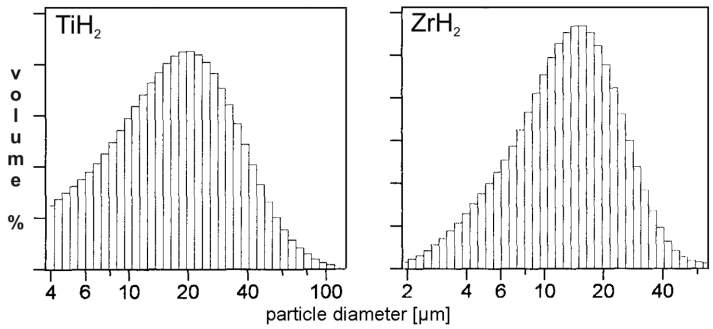

Fig. 2. Particle size distribution of the TiH_2 and ZrH_2 powders used for foaming Zn measured by laser diffraction.
Mean particle size of TiH_2 is 22.35 µm, that of ZrH_2 14.75 µm

2 Zinc foam

2.1 Blowing agent size distribution

Our first investigation aimed at the size distribution of the blowing agent. Two powders were used: TiH_2 and ZrH_2. For TiH_2 two batches were created by sieving, with particle sizes below and above 28 µm. From laser diffraction size analysis we know that the mean diameter of unsieved TiH_2 is 22.35 µm, that of ZrH_2 14.75 µm (see also Fig. 2).

Tomographic images of unfoamed zinc precursor with TiH_2 were taken (not foam - it is nearly impossible to distinguish between TiH_2 and the metal/air interface due to nearly identical attenuation coefficients). Separation of the blowing agent information and plain voxel counting delivers a plot of the volume fraction (in percent) versus the particle diameter. Assuming spherical particles, the diameter D can be calculated from the volume V (voxel count times voxel volume) as $D=(6V/\pi)^{1/3}$. In Fig. 3 (left image) the result is displayed for sieved powder with nominal particle sizes below 28 µm. As expected, a

clear maximum is found below 28 µm but surprisingly particles with diameters greater 28 µm appear with a significant volume fraction. We therefore conclude that during powder processing the original particle size distribution is lost due to agglomeration.

This is emphasised by the results for ZrH_2 particles (see right image in Fig. 3) determined from a tomographic image from a zinc foam. Here nearly all particles appear with a diameter much larger than the mean (14.75 µm) of the particle size analysis on loose powder.

Therefore, the particle size distribution of the blowing agent in powder compacts cannot be fully controlled by a simple selection of the powder. Agglomeration effects have to be kept in mind because they shift the particle size to higher values.

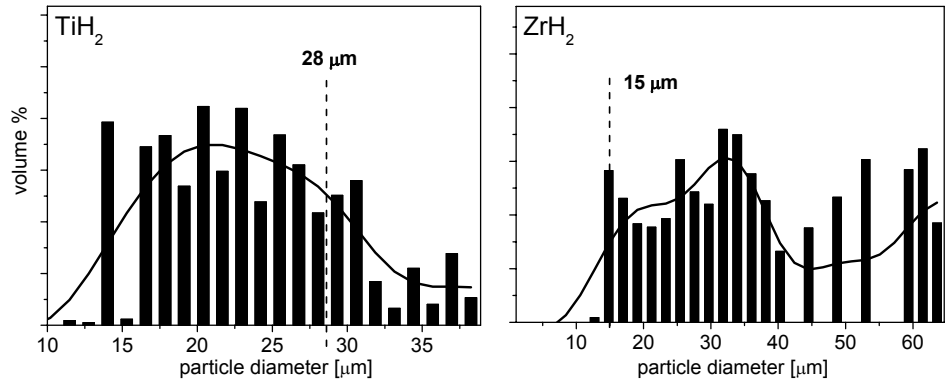

Fig. 3. Particle size distribution of blowing agent determined by tomography, left: sieved TiH_2 powder (size < 28 µm), right: ZrH_2 (unsieved)

2.2 Critical thickness of cell walls

Next we take a closer look at the parameters characterizing the foams. The critical thickness of cell walls at the moment of rupture has already been studied with X-ray radiography for aluminium foams. A value around 50 ± 10 µm was found [5].

With ex-situ tomography a detailed view inside the foam structure is obtained (see e.g. Fig. 1, left image). Pores in the final expansion stage can be found just by visual selection. The corresponding wall thickness can be obtained by simple voxel counting – a function already included in many commercial voxel displaying software packets. With this method we find the critical thickness of cell walls in zinc foams to range from 40 to 70 µm - the similar range as for aluminium foams. This is interesting as the viscosity for aluminium at its melting point (660 °C) is η_{melt}=1.25 mN/m^{2}s, three times smaller than for zinc (3.75 mN/m^{2}s) at its melting point (419 °C). This supports the conclusion that the viscosity close to the melting point does not have very much influence on foam stability expressed by the critical cell wall thickness. This is in accordance with prior observations [6].

2.3 Pore size distribution

Finally, the pore size distribution in zinc foam is examined. In contrast to aluminium foam, where a pore size distribution with a certain maximum is often found [1], zinc foam shows a different behaviour. A look at a tomographic image of zinc foam (see both images in Fig. 1 for a 2D slice) displays clearly that besides a pore population with large diameters a population with small pores also exists.

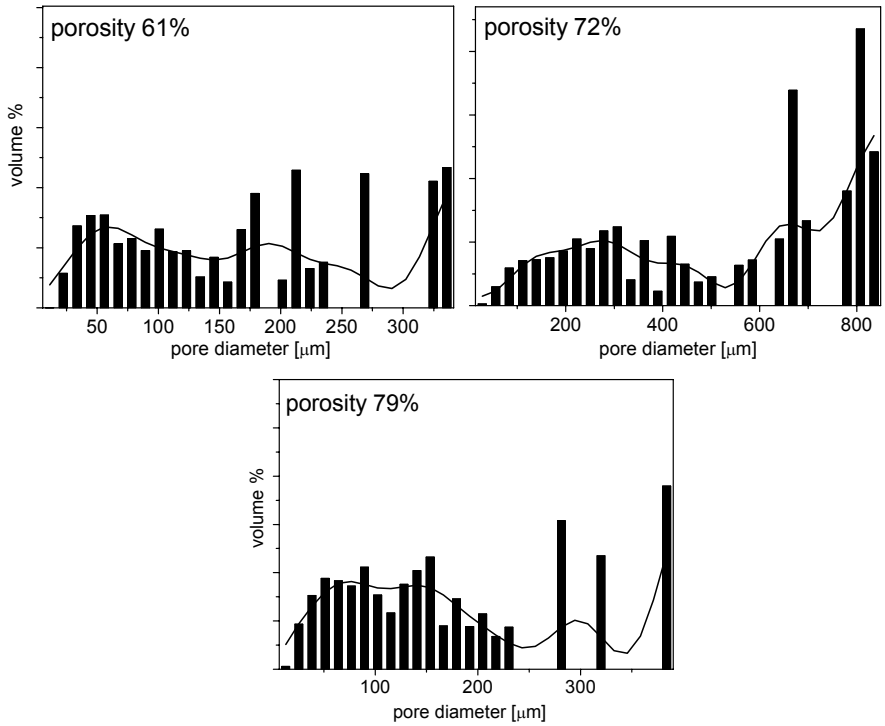

Fig. 4. Pore size distribution for zinc foam with different porosities

As with the blowing agents we assume the pores to be spherical and use $D=(6V/\pi)^{1/3}$ again to calculate the diameter from the pore volume. With plain voxel counting and this formula we calculate the pore size distributions for different porosities (foaming stages) as displayed in Fig. 4.

All distributions have a significant broad maximum for pores with a small diameter. The samples investigated with synchrotron tomography are usually rather small – around $3\times3\times1.5$ mm^3 in our case. Therefore, our statistics for big pores are not satisfying especially for foams with higher porosities. Nevertheless (see also the pores in Fig. 1, right image) the pore size distribution in zinc foam is undoubtedly bimodal since it features two maxima. The small pores form a kind of satellite structure in the cell walls of the large ones.

The solubility of hydrogen in liquid zinc at a temperature close to the melting point is two orders of magnitude smaller than for liquid aluminium (< 0.002 at 516 °C for liquid zinc and 0.69 at 660 °C for liquid aluminium – measured in units of cm^3 of gas at

atmospheric pressure and 0 °C per 100 g metal [7]). A possible explanation for the different pore distributions in zinc and aluminium foam is based on this difference. In liquid aluminium very small pores cannot survive as the hydrogen is under a large pressure ($p \propto 1/\text{diameter}$) and easily escapes. Therefore, we have a minimum pore size at which an equilibrium between pressure and diffusion exists. For the zinc foam the hydrogen is trapped in each pore due to the small solubility and therefore smaller pores can survive.

3 Aluminium foam

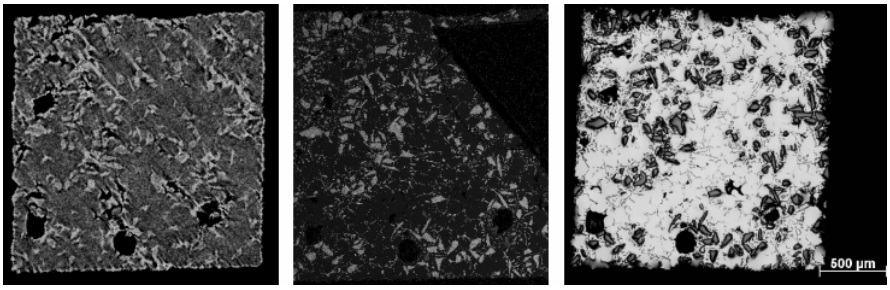

Fig. 5. Left: non-destructive tomographic slice of aluminium foam (grey = aluminium matrix, white = TiH_2, light grey = SiC), middle: SEM-EDX composition analysis on the corresponding polished section (same color-code), right: corresponding light microscopic image of the section.

Aluminium foams have to be stabilised with SiC when they do not contain enough oxides. The question is whether the SiC particles are really located next to pore surfaces and which mechanisms are responsible for such a correlation if it exists. Investigations via EDX analysis are always limited to 2D information and are insufficient.

Aluminium (AlSi10Mg) foams have been investigated by tomography (see Fig. 5). The attenuation coefficients of aluminium (μ=5.0 cm^{-3}) and SiC (μ=5.7 cm^{-3}) are very similar leading to a very small absorption contrast in the tomographic images (see Fig. 5). In order to verify our results we prepared one slice we found in a tomographic image for composition analysis by EDX in a SEM and also for light microscopy. The result is displayed in Fig. 5. One can see that the three methods yield the same morphological and chemical structure. By using synchrotron tomography we therefore achieve a 3D image containing information about mass and chemical structure in a reliable way.

Images were separated into pores and SiC as described in the introduction. After this the correlation algorithm was applied. The result is displayed in Fig. 6. For the aluminium precursor a slight correlation (decreasing SiC density, black circles) is found in the neighbourhood of the pores (volume fraction 0 – 0.35) while for most of the bulk (volume fraction 0.35 – end) one finds no correlation (constant SiC density, dashed ellipse) as expected (Fig. 6, left). The first is due to the fabrication process where TiH_2 particles are added to a Al-SiC melt. Small initial pores appear where SiC particles can already locate themselves before the real foaming process starts. In addition, due to surface scattering the voxels on the boundary of each cell are counted as SiC particles. Fortunately, a strong correlation (decreasing SiC density, dotted ellipse) between the SiC particles and the pores can be seen in the plot for aluminium foam (Fig. 6, right). Therefore, the SiC particles migrate towards the pore surface during the foaming process.

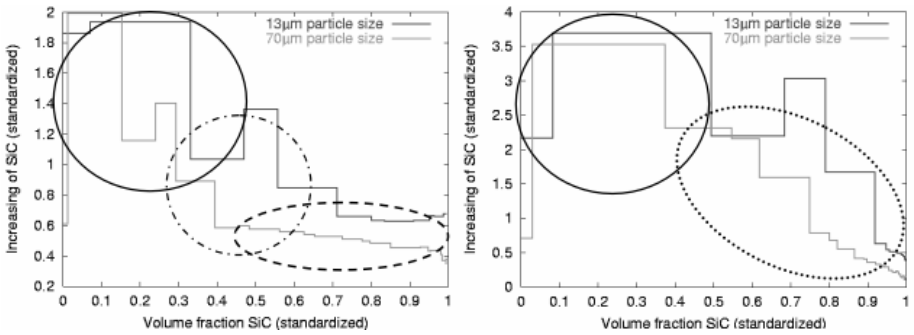

Fig. 6. Results of the correlation algorithm for the aluminium precursors (left) and the aluminium foam (right) for different SiC particle sizes

4 Summary

Our investigations on zinc and aluminium foams with synchrotron tomography delivered information about their 3D structure. Zinc foams have a bimodal pore size distribution probably due to the small hydrogen solubility of zinc. Despite the large difference in viscosity at the melting points of aluminium and zinc the critical cell wall thickness of both foams is in the same range. Therefore, viscosity does not play an important role for foam stability. For the blowing agent in zinc foams we found their size distribution to be effected by powder processing. The size of the particles is shifted to higher values due to agglomeration. For aluminium foams a clear spatial correlation between pores and SiC particles is shown. Further investigations about the mechanisms leading to this correlation are in work, some reports can be found in [8].

We acknowledge Lukas Helfen, Tilo Baumbach and Joachim Ohser for the support on the data analysis algorithms and helpful discussions, Vlado Gergely of the Department of Material Science of the University of Cambridge for the precursor materials and the Federal Institute of Materials Research and Testing (BAM) for experimental support.

References

[1] L. Helfen, T. Baumbach, H. Stanzivk, J. Banhart, A. Elmoutaouakkil and P. Cloetens, *Advanced Engineering Materials* **4**, (2002), 808-813
[2] J. Banhart, *Progress in Materials Science* **46**, 559-632 (2001)
[3] V. Gergely, B. Clyne, *Advanced Engineering Materials* **2**, 175-178 (2000)
[4] L. Helfen, H. Stanzick, J. Ohser, K. Schladitz, P. Pernot, J. Banhart and T. Baumbach, proceeding of the SPIE SS/NDE conference (2003)
[5] H. Stanzick, M. Wichmann, J. Weise, L. Helfen, T. Baumbach and J. Banhart, *Advanced Engineering Materials* **4**, (2002), 814-823
[6] T. Wübben, H. Stanzick, J. Banhart, S. Odenbach, *Journal of Physics: Condensed Matter* **15**, S427-S433 (2003)
[7] C. J. Smithells, E. A. Brandes, *Metals Reference Book*, Butterworth London & Boston, 1976
[8] A. Haibel, A. Rack, J. Banhart, proceedings of the International Symposium on Computed Tomography and Image Processing for Industrial Radiology (in press 2003)